PASA...14

Driftscan Surveys in the 21 cm Line with the Arecibo and Nançay Telescopes

F. H. Briggs,[1] E. Sorar,[2] R. C. Kraan-Korteweg[3] and W. van Driel[4]

[1]Kapteyn Astronomical Institute, Postbus 800, 9700 AV Groningen, The Netherlands
fbriggs@astro.rug.nl
[2]University of Pittsburgh, Pittsburgh, PA 15260, USA
[3]DAEC, Observatoire de Paris-Meudon, 92195, Meudon Cedex, France
[4]USN, Observatoire de Paris-Meudon, 92195, Meudon Cedex, France

Abstract: Driftscan methods are highly efficient, stable techniques for conducting extragalactic surveys in the 21 cm line of neutral hydrogen. Holding the telescope still while the beam scans the sky at the sidereal rate produces exceptionally stable spectral baselines, increased stability for RFI signals, and excellent diagnostic information about system performance. Data can be processed naturally and efficiently by grouping long sequences of spectra into an image format, thereby allowing thousands of individual spectra to be calibrated, inspected and manipulated as a single data structure with standard tools that already exist in astronomical software. The behaviour of spectral standing waves (multi-path effects) can be appraised and excised in this environment, making observations possible while the Sun is up. The method is illustrated with survey data from Arecibo and Nançay.

Keywords: methods: data analysis — techniques: image processing telescopes — surveys — galaxies: distances and redshifts — radio lines: galaxies

1 The Technique

The designs of the Arecibo and Nançay telescopes make them particularly well suited to taking data in a driftscan mode. Both have large collecting areas and are therefore sensitive survey instruments. They obtain the large collecting area by having much of their structure fixed to the ground. When they are used to track specific celestial coordinates, the on-axis gain changes and the far-out sidelobes move in unpredictable ways, causing spillover on the ground and RFI to be time-variable. These instabilities increase the level of systematic uncertainties, thus increasing the difficulty of detecting weak signals. Driftscan observations avoid these problems since all components of the structures are fixed relative to the ground, thus achieving the full sensitivity of the large reflecting areas. Similar arguments apply to more conventional radio telescopes, when variation in the spillover causes fluctuations in the spectral baselines and when RFI entering the receiving system is modulated by gain variations in the far sidelobes as the antenna tracks celestial sources. This report is based on experience obtained in extragalactic H I surveys using the Arecibo and Nançay Telescopes.

Sorar (1994) and Briggs conducted the Arecibo H I Strip Survey in the driftscan mode in order to determine the H I mass function for nearby extragalactic objects by surveying long strips at constant declination. The observations covered approximately 6000 independent sightlines to a depth of 7500 $km\,s^{-1}$, but since the strips were retraced on many days in order to increase the integration time on each sightline, nearly a million individual spectra had to be calibrated, regrouped and averaged. The details of the observational technique were developed by Sorar (1994), and the results and follow-up to the survey are summarised by Zwaan, Sprayberry & Briggs (1997, present issue p. 117).

The method is also in use for surveys at Nançay. One project, being conducted by Kraan-Korteweg, van Driel, Binggeli and Briggs, will test the completeness to a depth of 2300 $km\,s^{-1}$ of deep optical catalogs of dwarfs and low surface brightness galaxies in the CnV I cloud (Binggeli, Tarenghi & Sandage 1990). A sample of the raw data from the H I survey is shown in Figure 1. The spectral passband calibration for these data has been performed by computing the average spectrum of the entire 3·5 hour dataset, and each spectrum was divided by the average spectrum as it was loaded in time sequence into the columns of the image. Passage of a telescope beam over a background continuum source is registered in the image as a dark band. The residual Galactic H I emission causes the splotchy horizontal band across the image around the H I rest frequency.

34d 27'

15h 00m   Right Ascension   11h 30m
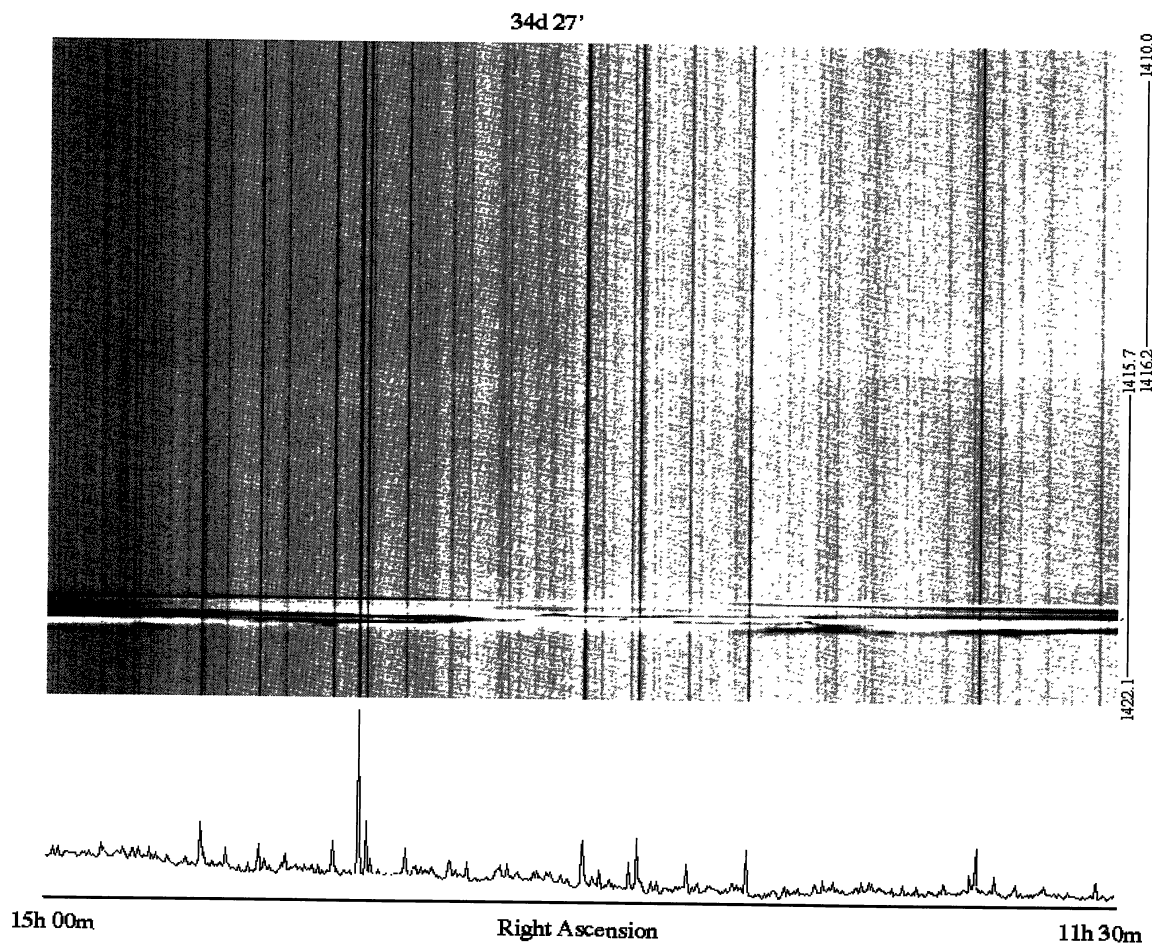
Figure 1—Nançay raw data image. Passband-calibrated spectra have been loaded into the image in time sequence increasing from right to left. There are two slightly overlapping, 6·4 MHz wide spectral bands, as marked at the right border. A trace of the continuum as a function of right ascension is drawn under the image.

Once the data are loaded in image format, images become the units in which the data are stored, manipulated and displayed. For example, continuum subtraction, averaging of data from different days and smoothing can be accomplished using procedures in familiar astronomical image processing packages. Figure 2 shows the processed spectra for a total of ~2500 sightlines in three adjacent declination strips. The figure results from approximately 82 000 individual spectra. There are 11 detected extragalactic signals resulting from 9 separate galaxies, plus a number of interesting features associated with Galactic H I.

A second project now in progress at Nançay will observe ~6% of the sky to a depth of 4500 km s^{-1} with noise level ~23 mJy (5σ) for velocity resolution 20 km s^{-1}. The survey is well matched to detecting nearby examples of gas-rich systems such as H I 1225+01 (Giovanelli & Haynes 1989; Chengalur, Giovanelli & Haynes 1995) and the circum-galactic ring in Leo (Schneider 1989), as well as detecting a sample of several hundred normal galaxies.

2 Spectral 'Standing Waves'

Faint periodic fluctuations in the background noise are visible in the low-velocity ranges of each strip in Figure 2. These are commonly called 'standing waves' by radio spectroscopists. In these Nançay data, they occur in the correlator quadrants that have strong Galactic H I emission, but not in the higher-velocity quadrants. The standing waves arise because Galactic H I signal enters the receiving system by two paths of different lengths. In an ideal telescope this would not happen, but it is common in the present design of radio telescopes, since radiation entering the radio receiver may have been weakly scattered by structure that crosses the telescope's aperture; this additional scattering can deflect off-axis radiation into the beam of the telescope. When
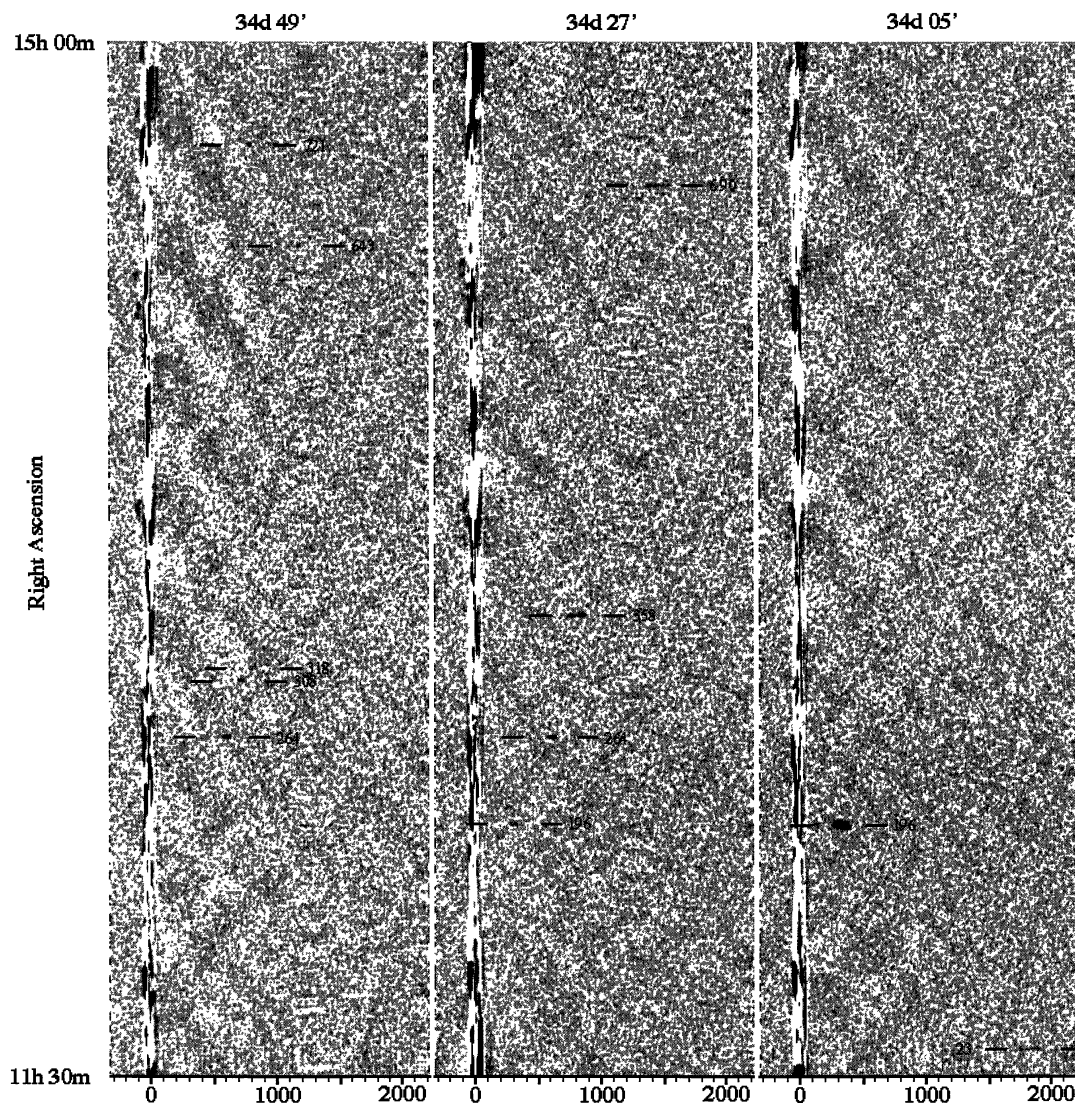
Figure 2—Processed Nançay images for three declinations. Spectra are loaded in horizontal lines in this image, with right ascension increasing upwards. Overlap of the spectral sub-bands has been removed, and labels on the horizontal axis indicate velocity in km s^{-1}. Eleven detected signals are marked.

two copies of a signal take different paths to the receiver, the signal taking the longer path suffers a delay, and when the autocorrelation function is computed in the spectrometer, a correlation spike is obtained in the delay channel corresponding to the extra pathlength. In the Fourier transformation of the ACF to obtain the power spectrum, a single-channel spike transforms to a sinusoidal variation across the band. Thus the path delay corresponds directly to the number of cycles of standing wave across the spectral band. For the high-velocity ranges of Figure 2, there is no interfering signal entering the system with a time delay and with sufficient strength to generate standing waves, and

therefore the noise characteristics in this redshift range are better behaved.

Any broadband signal entering the receiving system in multiple copies with different delays can give rise to these multipath effects. A strong source of such radiation is the Sun during daytime observations, but terrestrially generated broadband RFI, Galactic emission, strong radio continuum sources and spillover can also do it. The standing waves are often dominated by a single periodicity, representing, for example, a round trip delay between the feed cabin and the dish surface. However, a further complication is that antenna structures are often sufficiently complex that several scattering
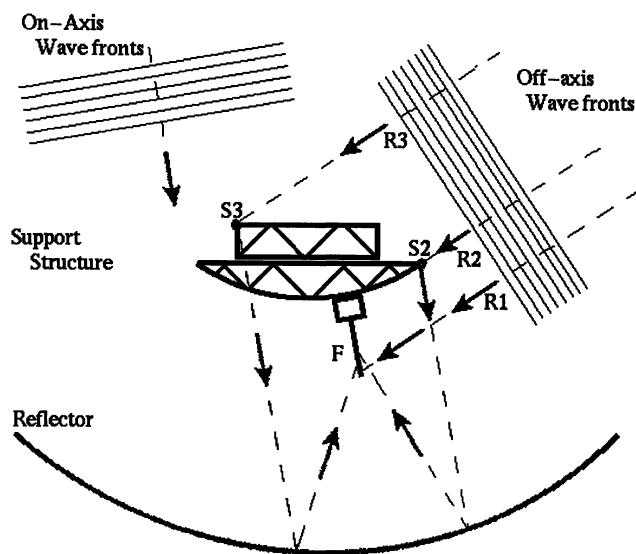
Figure 3—Schematic of multipath scattering at the Arecibo Telescope. Representative off-axis rays, R1, R2, and R, are seen traversing paths of different length before arriving at the Arecibo line feed F. In this diagram, R1 takes a direct path to the feed, while R2 and R3 are scattered from different points (S2 and S3) on the support structure. Radiation is actually scattered in many directions at the scattering points S2 and S3, but those rays that are scattered downward parallel to the incoming on-axis rays are directed to be optimally reflected from the main reflector directly toward the feed.
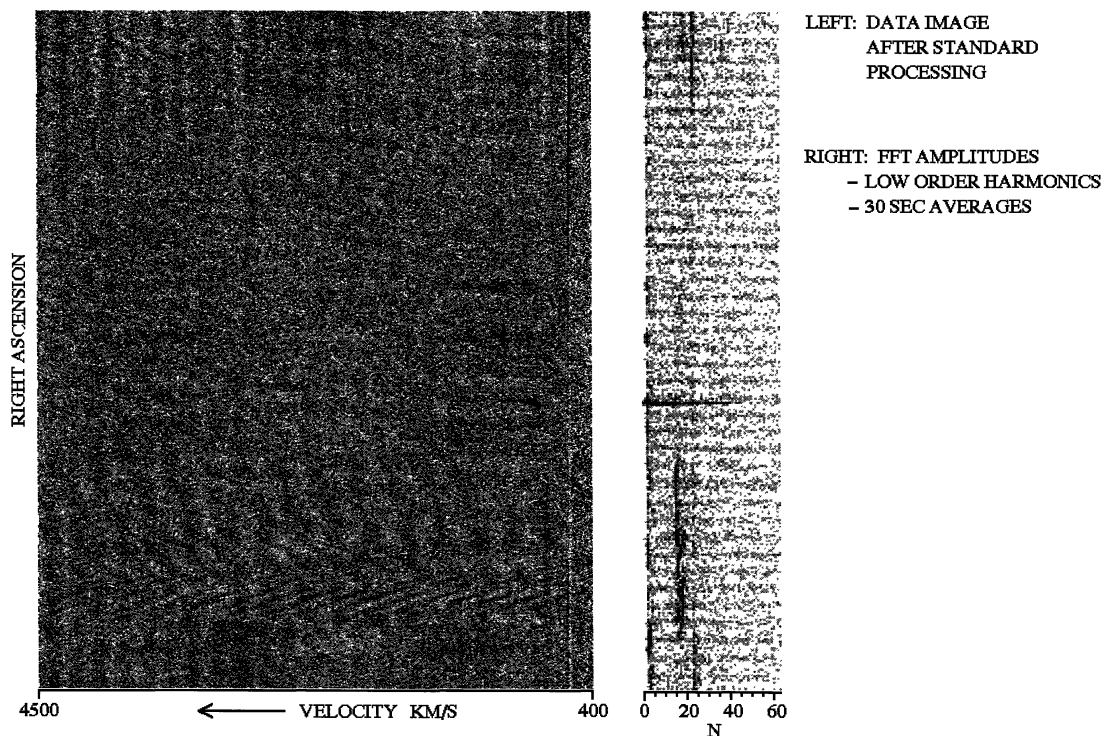

LEFT: DATA IMAGE
AFTER STANDARD
PROCESSING

RIGHT: FFT AMPLITUDES
– LOW ORDER HARMONICS
– 30 SEC AVERAGES

Figure 4—Arecibo daytime standing waves. (*Left*) The data image for a single circular polarisation after the standard calibration and continuum removal. The image contains 1250 seven-second time steps for a duration of ~2·4 hours. The bright, spatially resolved galaxy M94 can be seen midway through the image in the low-velocity range. There is a faint linear feature running vertically in the image at slightly lower velocity: this is Galactic H I emission that is aliased into the spectrum through the baseband filters. (*Right*) Harmonic content of each row in the image for the first 63 harmonics. The amplitudes have been averaged by 4 time steps in this image.
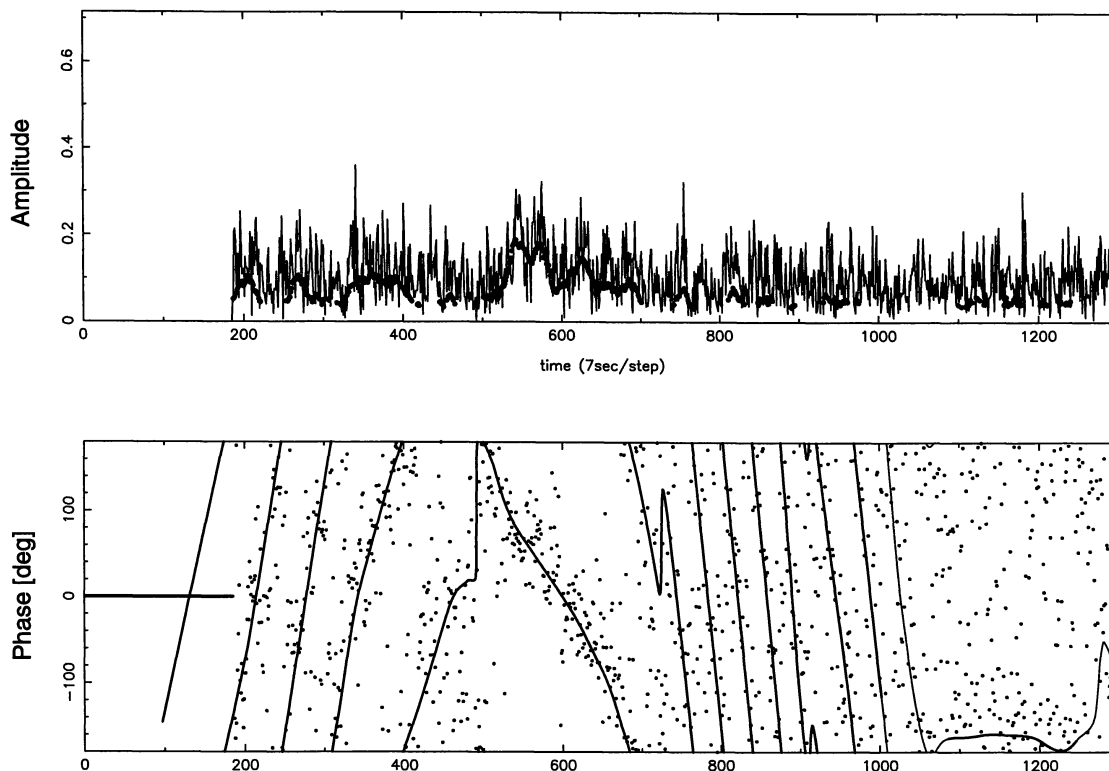
Figure 5—Amplitude and phase for the $n = 15$ harmonic standing wave. (*Top*) Coefficient amplitudes plotted as a function of time step (light noisy curve). The heavy solid points are vector averages of the amplitude (for 20 time steps), computed after application of the phase tracking algorithm. Heavy points are plotted only when the amplitude surpasses a set threshold. (*Bottom*) Standing wave phases (points). Smooth interpolated curve results from the phase tracking algorithm. The curve is lighter in regions where the signal-to-noise ratio for the wave is low.

locations can contribute (as illustrated for the Arecibo Telescope in Figure 3), producing signals in several delay channels of the ACF. When the Fourier transform is computed, the spectral passband produced by the combination of multiple sinusoidal components can be very complicated. Figure 4 illustrates the complexity of standing wave patterns caused by the Sun in some Arecibo observations made during a late afternoon observation. Note that while the feed was positioned at the same antenna coordinates, this same pattern repeated on successive (solar) days. There was a slow change in the pattern after several days as the Sun moved in declination.

As well as varying in amplitude, standing waves can drift in phase with time, causing them to fail to subtract exactly when the simpler forms of passband calibration are applied. This is true of the processing that has been done to obtain Figure 2, and substantial residuals remain in the low-velocity range. There is a time range in the observations shown in Figure 4 where the drift is so rapid that the wave moves by a full turn of phase in just a few minutes. Fortunately, there is a straightforward way to tackle this problem and remove even these complicated patterns from

the driftscan data in an unbiased way. It begins by performing the Fourier transform of the power spectrum $S_{t_i}(\nu)$ to obtain the amplitudes and phases of the standing wave components during each time step t_i. These harmonics can be written as complex coefficients $\mathbf{A}_{n,t_i} = A_{n,t_i} \exp(i\phi_{n,t_i})$, where n labels the harmonic by the number of full periods of the wave across the spectral band and t_i indicates that the coefficients are expected to change with time, as the spectra are recorded in discrete time steps. In principle, the Fourier analysis of a string of real numbers, such as these spectra, produces one half as many complex harmonic coefficients as there were spectral channels in the power spectrum, but in practice, the standing waves arise from significant signal only at low values of n. Thus, the standing wave content of an image-formatted database can be described by another 'image' (or table) of complex numbers, with the same number of time steps, but many fewer values for $\mathbf{A}_n$ than are required for the number of channels in the spectrum $S(\nu)$.

Figure 4 shows the time behaviour of the harmonic content of the first 63 harmonics in the Arecibo data image in the left part of the figure. The standing waves appear with a variety of periodicities, with several long-lived bursts in the harmonics around

$n = 20$, which corresponds to differential delays of $\sim 1\,\mu$s, the round-trip light travel time between the Arecibo feed support structure and the surface of the reflector. There is substantial variability depending on where the scatterer is located on the support structure. There are also some bursts of signal in the lowest harmonics, possibly due to differential delays between scattered paths such as R3 and R2 in Figure 3, which are both scattered downward into the dish from different points on the support structure; alternatively, there could be scattering from point S2 directly in the direction of the feed F, which would also cause a fairly short differential delay and thus a long-period standing wave. The harmonic signature of a bright galaxy can also be seen near the midpoint of the data set. The faint, periodic, horizontal striping is a result of the slightly variable correlator dump time, causing the record integration time to beat with the 7 s grid spacing to which the data were interpolated.

Phase drift of an n harmonic standing wave is described by watching the phase term $\phi_n(t)$ from $\mathbf{A}_{n,t_i}$ vary with time. Figure 5 shows an example of the amplitude and phase data for a single harmonic $n = 15$. The time variation of both $A_n(t)$ and $\phi_n(t)$ can be efficiently tracked in time by sliding a window of 16 to 128 time steps along the table of $\mathbf{A}_{n,t_i}$ and then taking the Fourier transform of the complex time series of each harmonic within the windowed region.

A recipe for tracking and modelling a standing wave is summarised as follows:

(1) Compute the table (or image) of complex harmonic coefficients $\mathbf{A}_{n,t_i}$.

(2) Separate the complex coefficients of the nth harmonic as a function of time into a single long vector (such as the data plotted in Figure 5).

(3) Subdivide the vector into short enough time spans that the rate of drift is nearly constant over that time window. The choice of length for the time window depends on how rapidly the rate of drift changes, since the window must be short enough to track changes in the drift rate but also long enough to be immune to signals that are localised in a single beam. Of course, a choice for the window length of 2^N time steps (with N equal to an integer in the range 4 to 7) helps to increase the efficiency in computing the transform.

(4) The phase interpolation needed to track the waves is simplified if there is overlap of the windows, and therefore the window is advanced by either 2^{N-1} or 2^{N-2} time steps before recomputing the transform. Thus, a mathematical summary is: each window contains $p = 2^N$ points taken from $\mathbf{A}_{n,t_i}$ with t_i running from t_m to t_{m+p-1}. The Fourier transform of this series of p numbers produces p complex coefficients $\mathbf{a}_{n,\delta_k} = a_{n,\delta_k} \exp{(i\theta_{n,\delta_k})}$. Here a_{n,δ_k} is the strength of the component drifting at

rate δ_k with phase θ_{n,δ_k} at time $t_w = t_{m+p/2}$. In principle, there may well be a range of different standing wave drift rates δ contributing at any given time, since many locations on the support structure are capable of scattering. In practice, we select the strongest a_{n,δ_k} component in each time window, and tabulate δ_k and θ_{n,δ_k} after checking for significance relative to the noise level.

(5) Depending of the degree of overlap of the windows, each time step t_i falls in either 2 or 4 windows. Each window that produced valid measurements for δ_k and θ_{n,δ_k} can be used to form an estimate of the standing wave phase at t_i. Thus, a reasonable method for tracking the phase for the nth harmonic is to compute an estimate $\langle \phi_{n,t_i} \rangle$ for the phase at each time from the weighted vector average of the overlapping windows:

$$\eta e^{i\langle \phi_{n,t_i} \rangle} =$$

$$\left[\sum W_{n,w}(|t_i - t_w|)^\rho e^{i(\delta_{k,w}(t_i - t_w) + \theta_{n,\delta_k,w})} \right]$$

$$\times \left[\sum W_{n,w}(|t_i - t_w|)^\rho \right]^{-1}.$$

The sums are taken over the 2 (or 4) windows that overlap at t_i. The weighting factors include $W_{n,w}$, which indicates the statistical significance of the solution for the window w, and a factor $(|t_i - t_w|)^\rho$, which gradually transfers the weight among the windows by assigning the greatest emphasis to the solution whose window is centred closest to t_i. The factor ρ is one of many possible weight adjustments. An amplitude η also results from the vector average; η is close to unity when there is close agreement between the phase determined by all the windows included in the average.

(6) Once a solution for phase tracking has been performed (such as that shown in the lower panel of Figure 5), a model for the temporal behaviour of the wave amplitudes can be made by smoothing the time sequence of $A_{n,t_i} \exp[i(\phi_{n,t_i} - \langle \phi_{n,t_i} \rangle)]$. When the resulting wave amplitudes surpass a set threshold for significance, they can be stored in a table of harmonic coefficients that can subsequently be used to generate models for the standing waves as a function of time (as shown in Figure 6) and then to correct the observations by subtracting the standing wave model from the data image. Note that this technique succeeds in doing little damage to the celestial signals, since galaxies typically fall in only one beam and the fits are derived from many beams. This approach is far superior to simply 'nulling' the $\mathbf{A}_n$ component, since this would throw away genuine information from the sky that is specific to each beam.

While our experience at Arecibo and Nançay has shown that the strongest standing waves are due to the Sun, we have also seen similar, but weaker,
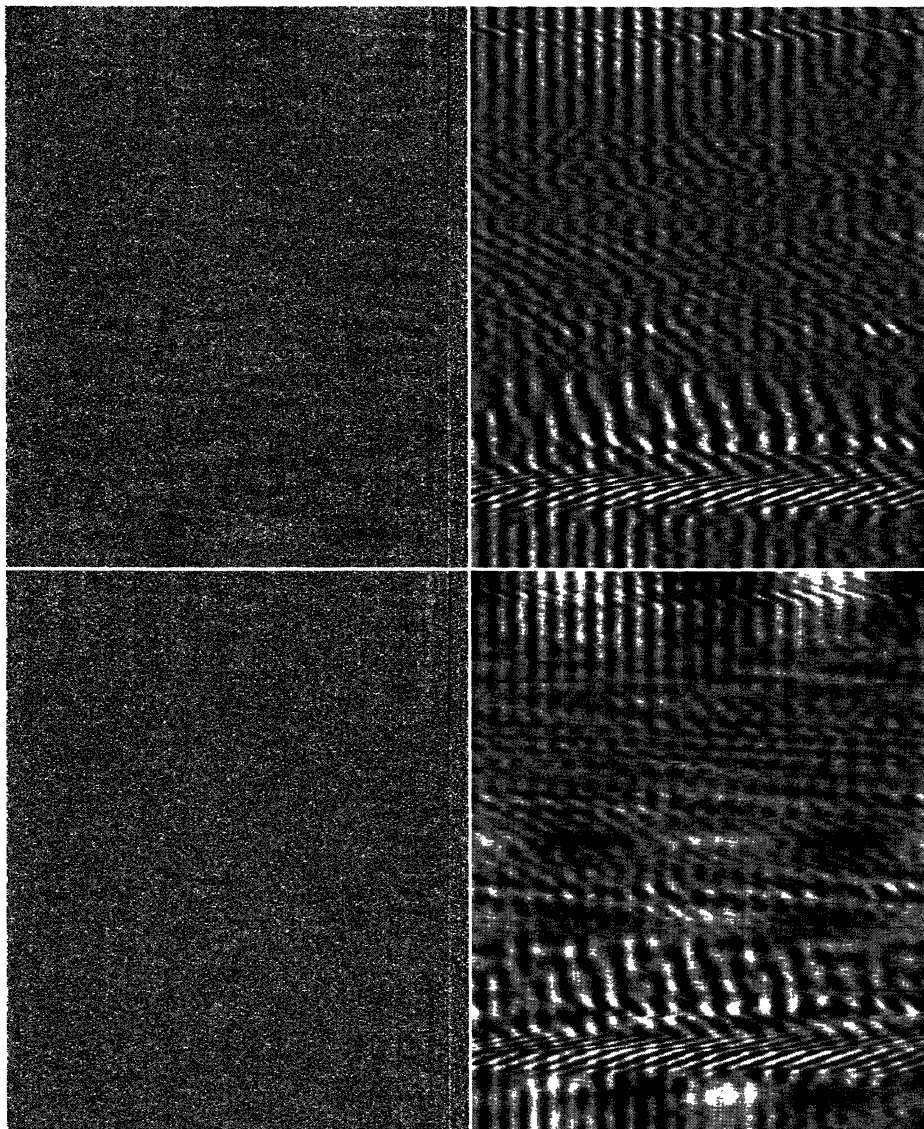
Figure 6—Standing wave edits. (*Left panels*) Versions of the data image in Figure 4, but with standing wave models subtracted. The data images are presented on the same greyscale wedge as Figure 4. (*Right panels*) Standing wave models built from harmonic analysis of the data image in Figure 4, followed by application of a phase tracking algorithm and reconstruction of noise-free images of the standing waves. The upper model includes harmonics $n = 4$ through 25, when they are deemed significant. The lower model includes $n = 1$ through 25. The greyscale is about three times more sensitive for the models than for the data images.

standing waves at night at Arecibo when observing in the vicinity of the strong radio source Taurus A (the Crab Nebula); in this case, the pattern repeated at the same sidereal time day after day. Very strong standing waves have also been generated by faulty equipment that generated intermittent, broadband noise; these waves had fixed phase in successive scans, since the source of the RFI was fixed to the

Earth and the antenna was stationary during the observation.

3 Final Comments

The driftscan technique for spectral line surveying offers a number of advantages over pointed observations: (1) Data quality is maximised since the telescope is still relative to the ground; spillover, far

sidelobes and on-axis gain are constant. (2) System stability can be monitored with high precision. (3) The observations are 100 per cent efficient since data can be taken continuously. (4) The telescope scheduling is simple, and observing staff have little real-time responsibility, since the telescope is sitting still with the brakes on. (5) Spectral passband fluctuations due to standing waves (or any other instability that varies on timescales longer than a few minutes) can be tracked and removed, permitting observations to be made during the daytime. (6) The data are naturally processed in image format; the analysis is very simple and efficient, and allows large projects to be tackled using existing software that is proven and familiar.

Acknowledgments

Binggeli, B., Tarenghi, M., & Sandage, A. 1990, A&A, 228, 42
Briggs, F. H. 1997, PASA, 14, 31
Chengalur, J. N., Giovanelli, R., & Haynes, M. P. 1995, AJ, 109, 2415
Giovanelli, R., & Haynes, M. P. 1989, ApJ, 346, L5
Schneider, S. E. 1989, ApJ, 343, 94
Sorar, E. 1994, Ph.D. Thesis, University of Pittsburgh
Zwaan, M., Sprayberry, D., & Briggs, F. H. 1997, PASA, 14, 117